Journal of Scientific Computing (2022) 93:42
https://doi.org/10.1007/s10915-022-01978-6

A Multipoint Flux Approximation with a Diamond Stencil and a Non-Linear Defect Correction Strategy for the Numerical Solution of Steady State Diffusion Problems in Heterogeneous and Anisotropic Media Satisfying the Discrete Maximum Principle

T. M. Cavalcante[1] · R. J. M. Lira Filho[1] · A. C. R. Souza[1] · D. K. E. Carvalho[2] · P. R. M. Lyra[2]

Received: 3 November 2021 / Revised: 12 May 2022 / Accepted: 10 August 2022 /
Published online: 21 September 2022

Abstract
In the present paper, we solve the steady state diffusion equation in 3D domains by means of a cell-centered finite volume method that uses a Multipoint Flux Approximation with a Diamond Stencil and a Non-Linear defect correction strategy (MPFA-DNL) to guarantee the Discrete Maximum Principle (DMP). Our formulation is based in the fact that the flux of MPFA methods can be split into two different parts: a Two Point Flux Approximation (TPFA) component and the Cross-Diffusion Terms (CDT). In the linear MPFA-D method, this split is particularly simple since it lies at the core of the original method construction. In this context, we introduce a non-linear defect correction, aiming to mitigate, whenever necessary, the contributions from the CDT, avoiding, this way, spurious oscillations and DMP violations. Our new MPFA-DNL scheme is locally conservative and capable of dealing with arbitrary anisotropic diffusion tensors and unstructured meshes, without harming the second order convergence rates of the original MPFA-D. To appraise the accuracy and robustness of our formulation, we solve some benchmark problems found in literature. In this paper, we restrict ourselves to tetrahedral meshes, even though, in principle, there is no restriction to extend the method to other polyhedral control volumes.

Keywords 3D diffusion problems · Heterogeneous and anisotropic media · Unstructured tetrahedral meshes · Discrete maximum principle (DMP) · MPFA-DNL

✉ T. M. Cavalcante
tulio.mcavalcante@gmail.com

[1] Department of Civil Engineering, Institute for Petroleum and Energy Research, UFPE, Room 541, Av. Arquitetura s/n, Recife, PE 50740-550, Brazil

[2] Department of Mechanical Engineering, UFPE, Recife, PE, Brazil

1 Introduction

Steady-state diffusion problems that arise in various engineering and physical fields, such as fluid flow in porous media or heat conduction problems, are modeled by an elliptic partial differential equation with diffusion coefficients that can be represented by heterogeneous, possibly discontinuous, anisotropic full tensors. These problems can be challenging for traditional numerical methods, such as the classical Two Point Flux Approximation (TPFA) Finite Volume Method (FVM), which is monotone [1], but it is not even convergent for general full tensor diffusion coefficients or general non k-orthogonal meshes [2–4]; the Galerkin Finite Element Method (GFEM) [5, 6], the Mixed-Finite Element Method (MFEM) [7, 8] or even the more robust linear Multipoint Flux Approximation (MPFA) [2–4] methods which are, in general, convergent, but can violate the Discrete Maximum Principle (DMP), giving birth to spurious oscillations for the scalar variable and erroneous fluxes for more pathological problems with strong anisotropy ratios or extremely distorted meshes [1, 9].

The efforts to overcome these limitations are not recent. The DMP compliance for finite elements approximations was addressed by Ciarlet and Raviart [10], Korotov et al. [11] and Burman and Ern [12]. Le Potier [13] presented a 2D non-linear FVM satisfying the maximum principle and Cancès et al. [14] presented a non-linear technique to correct a general FVM in order to respect the DMP. Pal and Edwards [15, 16] proposed flux-splitting strategies to improve the monotonicity and impose DMP for FVM. Chen et al. [17] have proposed their MPFA with enriched stencil (MPFA-E), in order to mitigate, but not necessarily eliminate, spurious oscillations. Kuzmin et al. [18] presented a nonlinear constrained finite element scheme, in which they perform an algebraic matrix splitting followed by a slope limiting to impose DMP. Other finite volume formulations using two-steps strategies, as those presented by Su et al. [19] and Zhao et al. [20] also presents good results in terms of honoring the DMP.

However, some of these methods do not have some desirable properties such as, for example, the capability to reproduce exactly piecewise linear solutions (Linearity Preserving—LP) or local conservation [21, 22]. One of the formulations that is locally conservative and LP is the MPFA that uses the so called diamond stencil (MPFA-D) [23–26]. However, the MPFA-D, in its original form, is not monotone and does not respect the DMP, since the weighting of the vertices unknowns does not necessarily form a convex combination. The idea of the present work is to modify the original MPFA-D to avoid spurious oscillations on solving steady-state diffusion problems keeping it locally conservative and LP. It is possible to modify the weighting strategy in order to get a monotone scheme [27, 28], but it could unmake the linearity preserving in this case. On the other hand, the way we perform the modification stems from the fact that the MPFA-D flux expression can be naturally split into two parts: the TFPA flux portion and the flux portion associated with the cross-diffusion terms (CDT). This flux splitting [15, 16, 29], separating the TPFA part as the "spurious oscillations-free" part, is followed by a CDT flux limiting [18]. Our method aims to limit the CDT flux whenever it is necessary, in order to obtain monotone solutions, but keeping the modified MPFA-D as a locally conservative method and still capable of reproducing piecewise linear solutions, handling arbitrary (even discontinuous [30]) anisotropic diffusion tensors and achieving second order of accuracy on the scalar field and first order on its gradient.

In Sect. 2, we present the mathematical formulation, in Sect. 3, we present the discrete flux equations of the recently developed linear MPFA-D for 3D [26], followed by our new non-linear method designed to satisfy the DMP, i.e.: the Multipoint Flux Approximation with a Diamond Stencil and a Non-Linear Defect Correction (MPFA-DNL). In Sect. 4, aiming to appraise the accuracy and robustness of our new MPFA-DNL, we present the solution

of some 3D benchmark problems found in literature. In this paper, we restrict ourselves to unstructured tetrahedral meshes, even though, in principle, there is no restriction to extend our method to general polyhedral control volumes.

2 Mathematical formulation

The steady-state diffusion problem in 3D can be described by [26]:

$$\vec{\nabla} \cdot \vec{\mathcal{F}} = \mathcal{Q}(\vec{x}), \quad \text{with } \vec{\mathcal{F}} = -\mathbf{K}(\vec{x})\nabla u \text{ in } \vec{x} = (x, y, z) \in \Omega \subset \mathbb{R}^3 \tag{1}$$

in which $\vec{\mathcal{F}}$ represents the diffusive flux, u is the scalar or potential variable, $\mathcal{Q}(\vec{x})$ is the source term and $K(\vec{x})$ is the diffusion tensor that satisfies the ellipticity condition [31, 32] and that can be written, in Cartesian coordinates, as:

$$\mathbf{K}(\vec{x}) = \begin{bmatrix} \kappa_{xx} & \kappa_{xy} & \kappa_{xz} \\ \kappa_{yx} & \kappa_{yy} & \kappa_{yz} \\ \kappa_{zx} & \kappa_{zy} & \kappa_{zz} \end{bmatrix} \tag{2}$$

Moreover, appropriate boundary conditions can be defined by:

$$\begin{cases} u = g_D & \text{on } \Gamma_D \\ \vec{\mathcal{F}} \cdot \vec{n} = g_N & \text{on } \Gamma_N \end{cases} \tag{3}$$

where the scalar functions g_D (prescribed values for u) and g_N (prescribed fluxes) are, respectively, defined on Γ_D (Dirichlet) and Γ_N (Neumann) boundaries, with $\partial\Omega = \Gamma_D \cap \Gamma_N$ and $\Gamma_D \cap \Gamma_N = \emptyset$, and $\vec{n}$ is the unitary outward normal vector.

3 Numerical Formulation

In this section, from de the recently developed MPFA-D in 3D, we present our new MPFA-DNL, which includes a nonlinear defect correction strategy to the original MPFA-D formulation in order to satisfy the Discrete Maximum Principle (DMP) for unstructured tetrahedral meshes and general diffusion tensors.

Given a computational domain Ω with boundary Γ, we discretize it by a set of non-overlapping control-volumes $\hat{L}$. By integrating Eq. (1) and applying the Gauss's Divergence Theorem over the control-volume $\hat{L}$ (with boundary $\Gamma_{\hat{L}}$ and volume $\Omega_{\hat{L}}$), we have:

$$\int_{\Gamma_{\hat{L}}} \vec{\mathcal{F}} \cdot \vec{n} \partial\Gamma_{\hat{L}} = \int_{\Omega_{\hat{L}}} \mathcal{Q} \partial\Omega_{\hat{L}} \tag{4}$$

By using the mean value theorem, we can write:

$$\sum\nolimits_{\bar{\not{F}} \in \Gamma_{\hat{L}}} \vec{\mathcal{F}} \cdot \vec{N}\big|_{\bar{\not{F}}} = \bar{\mathcal{Q}}_{\hat{L}} \Omega_{\hat{L}} \tag{5}$$

where $\bar{\mathcal{Q}}_{\hat{L}}$ is the mean source term in $\hat{L}$ and $\bar{\not{F}}$ is a face belonging to the set $\Gamma_{\hat{L}}$. In Eq. (5) different approximations for the flux expression $\vec{\mathcal{F}} \cdot \vec{N}$ produce different finite volume approximations [2–4, 17, 23, 33].

3.1 The Multipoint Flux Approximation using the Diamond Stencil

We start from the formulation presented by Lira Filho et al. [26], which is applicable to diffusion problems on 3D tetrahedral meshes, in which the unique flux expression through a face, considering the configuration shown in Fig. 1, is given by:

$$\vec{\mathcal{F}}\cdot\vec{N} = -\mathfrak{K}\left|\vec{N}\right|\left[\left(u_{\hat{R}} - u_{\hat{L}}\right) - \frac{1}{2}\mathfrak{D}_{JK}(u_J - u_I) + \frac{1}{2}\mathfrak{D}_{JI}(u_J - u_K)\right] \tag{6}$$

with:

$$\mathfrak{K} = \frac{K^n_{\hat{R}}K^n_{\hat{L}}}{h_{\hat{L}}K^n_{\hat{R}} + h_{\hat{R}}K^n_{\hat{L}}} \tag{7}$$

and:

$$\mathfrak{D}_{i,j} = \frac{\vec{\tau}_{i,j}, \overrightarrow{\hat{L}\hat{R}}}{\left|\vec{N}\right|^2} - \frac{1}{\left|\vec{N}\right|}\left(h_{\hat{L}}\frac{K^{t,i,j}_{\hat{L}}}{K^n_{\hat{L}}} + h_{\hat{R}}\frac{K^{t,i,j}_{\hat{R}}}{K^n_{\hat{R}}}\right); i, j = I, J, K \tag{8}$$

where:

$$\vec{\tau}_{i,j} = \vec{N}\times\overrightarrow{i,j}; K^n_{\hbar} = \frac{\vec{N}^T K_{\hbar}\vec{N}}{\left|\vec{N}\right|^2}; K^{t,i,j}_{\hbar} = \frac{\vec{N}^T K_k\vec{\tau}_{i,j}}{\left|\vec{N}\right|^2}; \hbar = L, R; i, j = I, J, K \tag{9}$$

In this formulation, the auxiliary vertex unknowns (u_I, u_J, u_K) must be interpolated as a weighting of the values of u at the cells sharing the respective node (I, J or K. We use the linearity-preserving interpolation strategy presented by Lira Filho et al. [26].

It is clear, according to Eq. (6), that $\vec{\mathcal{F}}\cdot\vec{N}$. can be split in two parts:

$$\vec{\mathcal{F}}\cdot\vec{N} = \left(\vec{\mathcal{F}}\cdot\vec{N}\right)_{TPFA} + \left(\vec{\mathcal{F}}\cdot\vec{N}\right)_{CDT} \tag{10}$$

with:

$$\left(\vec{\mathcal{F}}\cdot\vec{N}\right)_{TPFA} = -\mathfrak{K}\left|\vec{N}\right|\left(u_{\hat{R}} - u_{\hat{L}}\right) \tag{11}$$

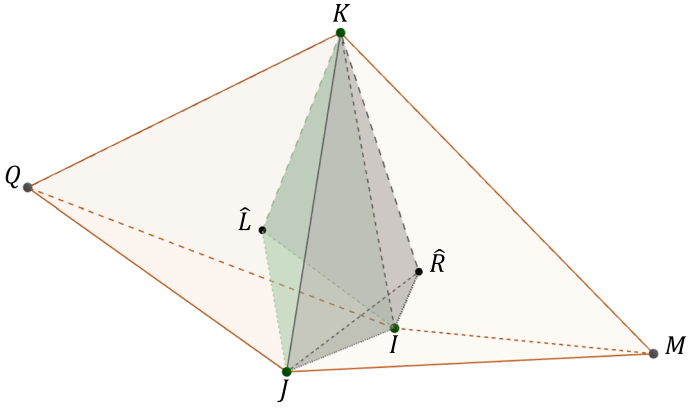

Fig. 1 Face ***IJK*** shared by the tetrahedrons $\hat{\boldsymbol{L}}$ and $\hat{\boldsymbol{R}}$

$$\left(\vec{\mathcal{F}}\cdot\vec{N}\right)_{CDT} = -\Re\left|\vec{N}\right|\left[-\frac{1}{2}\mathfrak{D}_{JK}(u_J - u_I) + \frac{1}{2}\mathfrak{D}_{JI}(u_J - u_K)\right] \tag{12}$$

where $\left(\vec{\mathcal{F}}\cdot\vec{N}\right)_{TPFA}$ is the TPFA flux contribution and $\left(\vec{\mathcal{F}}\cdot\vec{N}\right)_{CDT}$ is the flux contribution from the CDT, provided by the nodal interpolation.

Computing Eq. (5) for all the n control-volumes in Ω, we obtain the global system of equations $\boldsymbol{Au} = \boldsymbol{b}$. The solution of this system can be obtained iteratively by the Gauss–Seidel method:

$$\boldsymbol{u}^{t+1} = (\boldsymbol{D} + \boldsymbol{L})^{-1}\left\{\boldsymbol{b} - \boldsymbol{U}\boldsymbol{u}^{t}\right\} \tag{13}$$

where t is the iteration step and $\boldsymbol{D}$ is the diagonal matrix of $\boldsymbol{A}$, $\boldsymbol{U}$ is the upper triangular part of $\boldsymbol{A}$, $\boldsymbol{L}$ is the lower triangular part of $\boldsymbol{A}$, so that $\boldsymbol{A} = \boldsymbol{L} + \boldsymbol{D} + \boldsymbol{U}$. Naturally, $\boldsymbol{A}$ is a $n \times n$ matrix, in which the L-th line corresponds to $\sum_{\overline{k}\in\Gamma_{\hat{L}}} \vec{\mathcal{F}}\cdot\vec{N}\Big|_{\overline{k}}$. If we split the fluxes according to Eq. (10), we can write the global system of equations as:

$$[\boldsymbol{A}_{TPFA} + \boldsymbol{A}_{CDT}]\boldsymbol{u} = [\boldsymbol{b}_{TPFA} + \boldsymbol{b}_{CDT}] \tag{14}$$

in which the L-th line of $\boldsymbol{A_{TPFA}}$ corresponds to $\sum_{\overline{k}\in\Gamma_{\hat{L}}} \left(\vec{\mathcal{F}}\cdot\vec{N}\right)_{TPFA}\Big|_{\overline{k}}$ and the L-th line of A_{CDT} corresponds to $\sum_{\overline{k}\in\Gamma_{\hat{L}}} \left(\vec{\mathcal{F}}\cdot\vec{N}\right)_{CDT}\Big|_{\overline{k}}$, according to Eqs. (11) and (12). The expression shown in Eq. (14) is the regular MPFA-D global system under the described splitting. The solution of Eq. (14) can still be obtained iteratively by the Gauss–Seidel method, but in the following form:

$$\boldsymbol{u}^{t+1} = (\boldsymbol{D_{TPFA}} + \boldsymbol{D_{CDT}} + \boldsymbol{L_{TPFA}} + \boldsymbol{L_{CDT}})^{-1}\left\{\boldsymbol{b_{TPFA}} + \boldsymbol{b_{CDT}} - [\boldsymbol{U_{TPFA}} + \boldsymbol{U_{CDT}}]\,u^{t}\right\} \tag{15}$$

3.2 The Non-Linear Defect Correction

In this section, we present the Non-Linear Defect Correction strategy that we have devised to avoid the spurious oscillations that can arise with the use of the original linear MPFA-D method. After each iteration on Eq. (13), aiming to guarantee monotonicity through a local DMP imposition, we need to verify the compliance of the following restriction [16]:

$$\boldsymbol{u}^{t}_{\min} - \delta \leq \boldsymbol{u}^{t+1} \leq \boldsymbol{u}^{t}_{\max} + \delta \tag{16}$$

with the above inequality being an entry-by-entry comparison, where $\boldsymbol{u}^{t}_{\max}$ and $\boldsymbol{u}^{t}_{\min}$ are the vectors containing, respectively, the maximum and the minimum scalar values in the extended stencil of each cell after the t-th iteration and δ is a pre-established tolerance. The extended stencil of a cell includes the cell itself and all the neighboring cells sharing vertices with it. Two important exceptions to the application of Eq. (16) are when the evaluated cell has the maximum source term or the minimum sink term in the extended stencil or when it has Neumann boundary faces in which $g_N \neq 0$. In these cases, the restriction in Eq. (16) is simply skipped [16]. If the restriction shown in Eq. (16) is violated by the approximation, we need to modify the system shown in Eq. (15) in order to impose the DMP. As the potential

source of spurious oscillations in the MPFA-D are the fluxes associated to the CDT, we modify it as follows:

$$\boldsymbol{u}^{t+1} = (\boldsymbol{D_{TPFA}} + \Upsilon \boldsymbol{D_{CDT}} + \boldsymbol{L_{TPFA}} + \Upsilon \boldsymbol{L_{CDT}})^{-1} \left\{ \boldsymbol{b_{TPFA}} + \Upsilon \boldsymbol{b_{CDT}} - [\boldsymbol{U_{TPFA}} + \Upsilon \boldsymbol{U_{CDT}}] \boldsymbol{u}^t \right\} \tag{17}$$

where $\boldsymbol{\Upsilon}$ is a diagonal matrix, with entries $0 \leq \Upsilon_{ii} \leq 1$, used to weight the CDT contributions. Note that with $\boldsymbol{\Upsilon} = \boldsymbol{I}$ (the identity matrix), we get back to Eq. (15), i.e., the iterative version of the original MPFA-D, on the other hand, if $\boldsymbol{\Upsilon} = \boldsymbol{0}$, we get the iterative version of the TPFA formulation. Rearranging the expression above, we get:

$$\boldsymbol{u}^{t+1} = (\boldsymbol{D_{TPFA}} + \boldsymbol{L_{TPFA}} + \boldsymbol{\Upsilon D_{CDT}} + \boldsymbol{\Upsilon L_{CDT}})^{-1} \left[\boldsymbol{b_{TPFA}} - \boldsymbol{U_{TPFA}} \boldsymbol{u}^t + \boldsymbol{\Upsilon b_{CDT}} - \boldsymbol{\Upsilon U_{CDT}} \boldsymbol{u}^t \right] \tag{18}$$

Replacing Eq. (18) in Eq. (16) and disregarding the tolerance δ for now, we have the two following inequalities sets:

$$\begin{cases} (\boldsymbol{D_{TPFA}} + \boldsymbol{L_{TPFA}} + \boldsymbol{\Upsilon D_{CDT}} + \boldsymbol{\Upsilon L_{CDT}})^{-1} \left[\boldsymbol{b_{TPFA}} - \boldsymbol{U_{TPFA}} \boldsymbol{u}^t + \boldsymbol{\Upsilon b_{CDT}} - \boldsymbol{\Upsilon U_{CDT}} \boldsymbol{u}^t \right] \leq \mathrm{u}^t_{\boldsymbol{max}} \\ (\boldsymbol{D_{TPFA}} + \boldsymbol{L_{TPFA}} + \boldsymbol{\Upsilon D_{CDT}} + \boldsymbol{\Upsilon L_{CDT}})^{-1} \left[\boldsymbol{b_{TPFA}} - \boldsymbol{U_{TPFA}} \boldsymbol{u}^t + \boldsymbol{\Upsilon b_{CDT}} - \boldsymbol{\Upsilon U_{CDT}} \boldsymbol{u}^t \right] \geq \mathrm{u}^t_{\boldsymbol{min}} \end{cases} \tag{19}$$

Rearranging the system, we have:

$$\begin{cases} y_{\max} + \boldsymbol{\Upsilon} x_{\max} \geq 0 \\ y_{\min} + \boldsymbol{\Upsilon} x_{\min} \leq 0 \end{cases} \tag{20}$$

where:

$$\begin{aligned} x_{\max} &= U_{CDT} u^t + D_{CDT} \mathrm{u}^t_{\max} + L_{CDT} \mathrm{u}^t_{\max} - b_{CDT} \\ y_{\max} &= U_{TPFA} u^t + D_{TPFA} \mathrm{u}^t_{\max} + L_{TPFA} \mathrm{u}^t_{\max} - b_{TPFA} \\ x_{\min} &= U_{CDT} u^t + D_{CDT} \mathrm{u}^t_{\min} + L_{CDT} \mathrm{u}^t_{\min} - b_{CDT} \\ y_{\min} &= U_{TPFA} u^t + D_{TPFA} \mathrm{u}^t_{\min} + L_{TPFA} \mathrm{u}^t_{\min} - b_{TPFA} \end{aligned} \tag{21}$$

Therefore, we can determine valid intervals ($Y^i_{\max}$ and $Y^i_{\min}$) for the values of Υ_{ii}. Possible solutions to inequalities in Eq. (20) are given by:

$$Y^i_{\max} = \begin{cases} if\, x^i_{\max} > 0 \rightarrow \left[-\frac{y^i_{\max}}{y^i_{\max}}, \infty \right) \\ if\, x^i_{\max} < 0 \rightarrow \left(-\infty, -\frac{y^i_{\max}}{y^i_{\max}} \right] \\ if\, x^i_{\max} = 0 \rightarrow [0, 1] \end{cases} \tag{22}$$

and:

$$Y^i_{\min} = \begin{cases} if\, x^i_{\min} > 0 \rightarrow \left(-\infty, -\frac{y^i_{\min}}{x^i_{\min}} \right] \\ if\, x^i_{\min} < 0 \rightarrow \left[-\frac{y^i_{\min}}{x^i_{\min}}, \infty \right) \\ if\, x^i_{\min} = 0 \rightarrow [0, 1] \end{cases} \tag{23}$$

Therefore, we can define Y^i as:

$$Y^i = \begin{cases} if \quad \boldsymbol{u}^{t+1}_i \leq \mathrm{u}^t_{\min,i} \rightarrow Y^i_{\min} \cap [0, 1] \\ if \quad \boldsymbol{u}^{t+1}_i \geq \mathrm{u}^t_{\max,i} \rightarrow Y^i_{\max} \cap [0, 1] \\ else \rightarrow Y^i_{\max} \cap Y^i_{\min} \cap [0, 1] \end{cases} \tag{24}$$

If $Y^i = \emptyset$, we just adopt $Y^i = [0, 1]$, but not before taking an additional step. Consider that $\mathbb{V}$ is the set of violating DMP cells, if the $\hat{i} \in \mathbb{V}$ and $Y^i = \emptyset$, we include in $\mathbb{V}$ all the cells in the extended stencil of $\hat{i}$, so we can try to fix it through modifying its neighbors.

Note that, multiplying $\boldsymbol{\Upsilon A_{CDT}}$, which means to multiply the i-th line of $\boldsymbol{A_{CDT}}$ by Υ_{ii}, would be the same thing that multiply each face flux of the cell $\hat{i}$ by Υ_{ii}. This would violate the mass conservation. Considering a face $\overline{k}$ shared by two cells $\hat{R}$ and $\hat{L}$, as shown in Fig. 1, then the CDT flux through $\overline{k}$ is present in both L-th and R-th lines of $\boldsymbol{A_{CDT}}$. This way, through $\boldsymbol{\Upsilon A_{CDT}}$, the CDT flux through $\overline{k}$ would be multiplied by Υ_{LL} in the flux balance of $\hat{L}$ and by Υ_{RR} in the flux balance of $\hat{R}$. This would obviously destroy the flux continuity on $\overline{k}$. Therefore, it is necessary to determine a unique value α as the weighting factor to the cross-diffusion flux on each cell face as:

$$\alpha_{\overline{k}} \in F^k = Y^L \cap Y^R \tag{25}$$

On the other hand, if $F^k = \emptyset$, we perform a different procedure, in which we need to verify if there is any DMP violation at $\hat{L}$ or $\hat{R}$. If the DMP violation occurs only at $\hat{L}$, then $F^k = Y^L$. Analogously, if there is a DMP violation only at $\hat{R}$, then $F^k = Y^R$. However, if there is a DMP violation at both $\hat{L}$ and $\hat{R}$, we simply use $F^k = \left\{0.5\left[\min\left(Y^i\right) + \min\left(Y^j\right)\right], 0.5\left[\max\left(Y^i\right) + \max\left(Y^j\right)\right]\right\}$. For the case where there is no DMP violation, $F^k = [0, 1]$. Then the unique value of $\alpha_{\overline{k}}$ is defined as:

$$\alpha_{\overline{k}} = \begin{cases} if\ \max\left(F^k\right) < 1 \rightarrow \max\left(F^k\right) \\ if\ \max\left(F^k\right) = 1 \rightarrow 0.5\left[\min\left(F^k\right) + \max\left(F^k\right)\right] \end{cases} \tag{26}$$

Thus, we can see that as we have defined $\mathbb{V}$ as a set of cells violating DMP, we need to define a set of faces $\mathbb{F}$ whose CDT flux will be modified to avoid spurious solutions. This set will consist of all the faces comprising the cells in $\mathbb{V}$. Then, to formally guarantee flux continuity through a face $\overline{k} \in \mathbb{F}$, $\boldsymbol{A_{CDT}}$ must be corrected as follows:

$$\begin{cases} \boldsymbol{A}^{\hat{L}}_{\boldsymbol{CDT}} = \boldsymbol{A}^{\hat{L}}_{\boldsymbol{CDT}} + \left(\alpha_{\overline{k}} - 1\right)\left[\left(\vec{\mathcal{F}} \cdot \vec{N}\right)_{CDT}\Big|_{\overline{k} \in \mathbb{F}}\right] \\ \boldsymbol{A}^{\hat{R}}_{\boldsymbol{CDT}} = \boldsymbol{A}^{\hat{R}}_{\boldsymbol{CDT}} - \left(\alpha_{\overline{k}} - 1\right)\left[\left(\vec{\mathcal{F}} \cdot \vec{N}\right)_{CDT}\Big|_{\overline{k} \in \mathbb{F}}\right] \end{cases} \tag{27}$$

Evidently, $\boldsymbol{D_{CDT}}$, $\boldsymbol{U_{CDT}}$, $\boldsymbol{L_{CDT}}$ and $\boldsymbol{b_{CDT}}$ will be modified accordingly, because of the modification of $\boldsymbol{A_{CDT}}$. Since we compute $\alpha_{\overline{k}}$ explicitly, face by face in $\mathbb{F}$, these modifications may give rise to some undesirable side effects in other cells in terms of DMP violation. Therefore, the process described by Eqs. (21)–(27) is repeated, as shown in the algorithm in Fig. 2, until the condition in Eq. (16) is fulfilled. As it is well known that the classic linear TPFA method is a monotone formulation [34], we note that such a condition will be necessarily satisfied, at least in the extreme case in which $\Upsilon = 0$ and the CDT terms vanish. Thus, since we ensure the DMP in each iteration, the converged solution will undoubtedly satisfy the DMP. In the present paper we consider the solution converged when the iteration residue at the t-th iteration is $\mathfrak{r}_t < 10^{-3}\mathfrak{r}_1$, where $\mathfrak{r}_1$ is the first iteration residue, calculated from the initial guess u^0. Beyond this, we adopted $\delta = 10^{-6}$.

4 Results

In this section, we show the effectiveness of our non-linear formulation (MPFA-DNL) for the solution of some benchmark problems found in literature. Considering that the exact solution

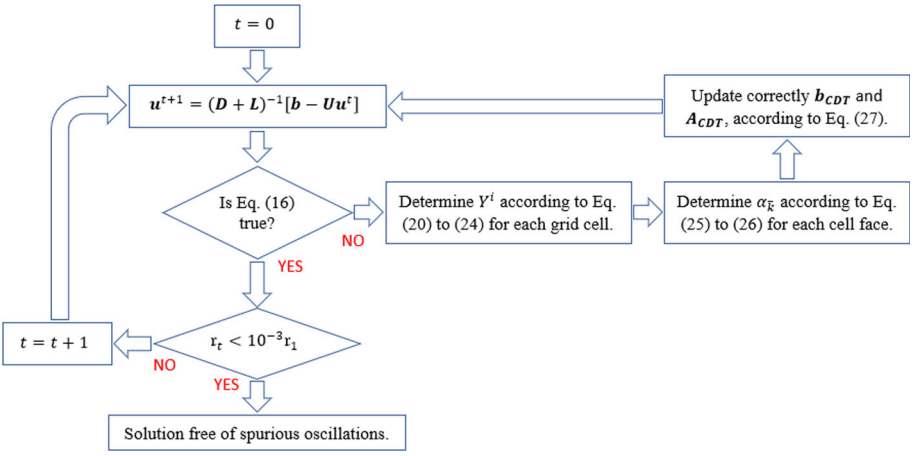

Fig. 2 The MPFA-DNL algorithm

is given by $\mathbb{U}$ and the approximate solution is represented by u, we can define the relative ℓ^2 norm of error for the scalar unknown u [26, 35] as:

$$\ell_u^2 = \sqrt{\frac{\sum_{i=1}^{n}(\mathbb{U}_i - u_i)^2\Omega_i}{\sum_{i=1}^{n}\mathbb{U}_i^2\Omega_i}} \tag{28}$$

and for its gradient ∇u as:

$$\ell_{\nabla u}^2 = \sqrt{\frac{\sum_{i=1}^{n}|\nabla\mathbb{U}_i - \nabla u_i|^2\Omega_i}{\sum_{i=1}^{n}|\nabla\mathbb{U}_i|^2\Omega_i}} \tag{29}$$

for which the numerical convergence rate is given by [35]:

$$q_{\mathfrak{z}} = -3\frac{\log\left(\frac{\ell_{\mathfrak{z},m}^2}{\ell_{\mathfrak{z},m-1}^2}\right)}{\log\left(\frac{n_m}{n_{m-1}}\right)} \tag{30}$$

for two successive meshes[1] ($m-1$ and m), with $m > 1$ and $\mathfrak{z} = u, \nabla u$. Furthermore, n is the total number of degrees of freedom of a mesh. We can also define the undershoot and overshoot norm of the error as [36]:

$$\varepsilon_m = \sqrt{\sum_{i=1}^{n}\left[\overset{2}{\max}(0, u_i - \mathbb{U}_{\max}) + \overset{2}{\max}(0, \mathbb{U}_{\min} - u_i)\right]\Omega_i} \tag{31}$$

where $\mathbb{U}_{\max}$ and $\mathbb{U}_{\min}$ are, respectively, the maximum and the minimum values for the solution defined by the boundary.

[1] The meshes we used can be found at the following address: https://github.com/tuliocavalcante/mesh.

4.1 Heterogeneous Diagonal-Anisotropic Media

We have manufactured this example to show that the MPFA-DNL corrects the DMP violation without degrading the numerical convergence rates of the MPFA-D. This problem has an analytic solution over the domain $\Omega = [0, 1]^3$, that implies in a non-homogeneous Dirichlet boundary condition on Γ_D, defined as:

$$u(x, y, z) = x(1 - x)y(1 - y)z(1 - z) \tag{32}$$

with an anisotropic diffusion tensor given by:

$$\mathbf{K} = \begin{bmatrix} x + 1 & 0 & 0 \\ 0 & y + 1 & 0 \\ 0 & 0 & 10(z + 1) \end{bmatrix} \tag{33}$$

and with a source term computed from using the definitions given by Eq. (32) and (33) in Eq. (1). In Tables 1 and 2, we can see the comparison between some results obtained with the MPFA-DNL and with the MPFA-D in its original (non-iterative) version. Table 1 shows how the MPFA-DNL is successful at avoiding the undershoots observed when we use the MPFA-D, what is reinforced by the norm ε_m.

Table 2 and Fig. 3, show that, despite the modifications performed by the non-linear defect correction approach on the original MPFA-D matrix, aiming to avoid the DMP violation, the

Table 1 Results for the test 4.1—heterogeneous diagonal-anisotropic media

	MPFA-D		MPFA-DNL	
n	$u_{\min}$	ε_m	$u_{\min}$	ε_m
215	3.72e−04	0	3.72e−04	0
2003	1.61e−05	0	1.62e−05	0
3898	− 6.43e−05	1.42e−6	7.63e−06	0
7711	− 3.99e−05	7.00e−7	2.26e−07	0
15,266	− 5.01e−05	4.55e−7	4.04e−07	0
30,480	− 3.36e−05	2.69e−7	1.29e−06	0

Table 2 Results for the test 4.1—heterogeneous diagonal-anisotropic media

	MPFA-D				MPFA-DNL			
n	ℓ_u^2	q_u	$\ell_{\nabla u}^2$	$q_{\nabla u}$	ℓ_u^2	q_u	$\ell_{\nabla u}^2$	$q_{\nabla u}$
215	0.210	–	0.585	–	0.209	–	0.585	–
2,003	0.044	2.113	0.284	0.971	0.042	2.147	0.284	0.972
3,898	0.027	2.203	0.236	0.828	0.025	2.306	0.236	0.830
7,711	0.017	2.082	0.176	1.299	0.015	2.313	0.176	1.298
15,266	0.011	1.964	0.144	0.880	0.009	2.055	0.144	0.879
30,480	0.007	2.086	0.113	1.038	0.006	1.730	0.113	1.035

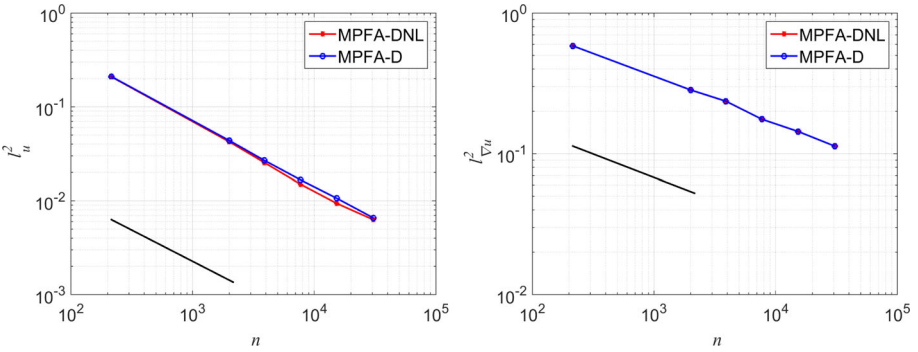

Fig. 3 The mesh convergence graphs for the test 4.1–Heterogeneous Diagonal-Anisotropic Media: on the scalar variable (left) and on its gradient (right)

convergence rates of our the MPFA-DNL method are not degraded. In fact, for certain meshes the errors were slightly smaller for the MPFA-DNL when compared to the original linear MPFA-D method.

4.2 Anisotropic Hollow Domain

Now, we consider the problem proposed by Danilov and Vassilevski [37]. In this problem, we consider a cubic domain $\Omega = [0, 1]^3$ with a central cubic hole $\Omega_h = [0.4, 0.6]^3$. At the external boundary $\partial\Omega$, the scalar variable is set as $u_e = 0$ and, at the internal edge $\partial\Omega_h$, the scalar variable is set as $u_i = 2$.

The anisotropic diffusion tensor is defined as:

$$\mathbf{K} = R_z^T R_y^T R_x^T \begin{bmatrix} 100 & 0 & 0 \\ 0 & 10 & 0 \\ 0 & 0 & 1 \end{bmatrix} R_x R_y R_z \tag{34}$$

where:

$$R_x = \begin{bmatrix} 1 & 0 & 0 \\ 0 & \cos\theta & -\sin\theta \\ 0 & \sin\theta & \cos\theta \end{bmatrix}; R_y = \begin{bmatrix} \cos\beta & 0 & \sin\beta \\ 0 & 1 & 0 \\ -\sin\beta & 0 & \cos\beta \end{bmatrix}; R_z = \begin{bmatrix} \cos\delta & -\sin\delta & 0 \\ \sin\delta & \cos\delta & 0 \\ 0 & 0 & 1 \end{bmatrix} \tag{35}$$

with $\theta = \pi/3$, $\beta = \pi/4$ and $\delta = \pi/6$. Results for both, the linear MPFA-D and the MPFA-DNL are shown in Table 3. In this table, we can see that the MPFA-D violates the DMP for all the tested meshes. On the other hand, the MPFA-DNL keeps the solution within the limits defined by the boundary conditions. In Fig. 4, we can see the scalar variable field at $y = 0.5$. As it can be seen, the MPFA-DNL clearly produces a smooth solution without spurious oscillations even for this test case in which we have a highly anisotropic diffusion tensor while the linear MPFA-D produces solutions with both, under and overshoots for almost all meshes used.

Table 3 Results for the test 4.2—anisotropic hollow domain

	MPFA-D			MPFA-DNL		
n	$u_{\min}$	$u_{\max}$	ε_m	$u_{\min}$	$u_{\max}$	ε_m
760	− 0.779	1.750	0.086	1.30e−5	1.706	0
1,660	− 0.537	2.070	0.049	0	1.975	0
2,193	− 0.307	1.907	0.029	0	1.896	0
4,471	− 1.054	1.976	0.065	0	1.926	0
10,552	− 0.868	2.239	0.026	0	1.966	0
17,544	− 18.59	21.91	0.585	0	1.968	0

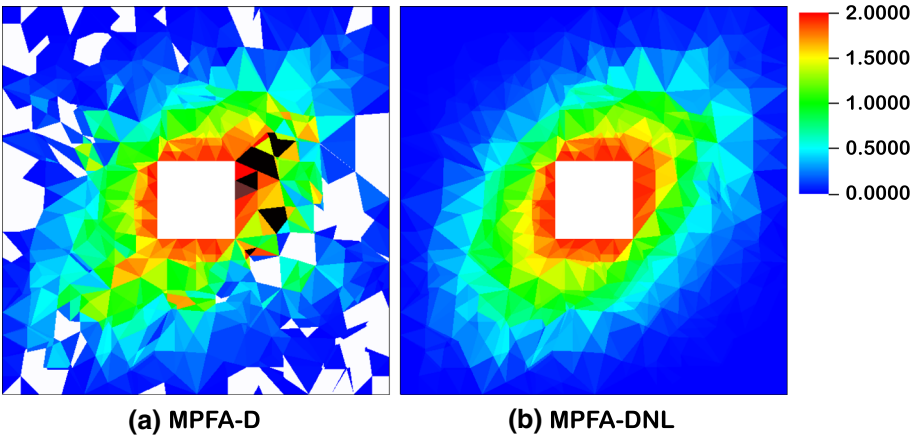

Fig. 4 Scalar variable field on the mesh with 17,544 tetrahedra, at $\boldsymbol{y} = 0.5$, for test 4.2–Anisotropic Hollow Domain. **a** Solution with the linear MPFA-D method. **b** Solution with the new MPFA-DNL. The black regions within the domain indicate overshoots for the scalar variable and the white regions indicate undershoots for the scalar variable

4.3 Two-Halves Anisotropic Hollow Domain

Finally, in the last example, we have devised a 3D example based on the 2D one from Queiroz et al. [36]. In this problem, we consider a cubic domain $\Omega = [0, 1]^3$ with a central cubic hole $\Omega_h = [0.4, 0.6]^3$. At the external boundary, $\partial\Omega$, the scalar variable is set as $u_e = 0$ and at the internal edge, $\partial\Omega_h$, the scalar variable is set as $u_i = 2$. The heterogeneous, discontinuous and anisotropic diffusion tensors are defined as:

$$\mathbf{K}_1 = R_z^T R_y^T R_x^T \begin{bmatrix} 100 & 0 & 0 \\ 0 & 10 & 0 \\ 0 & 0 & 1 \end{bmatrix} R_x R_y R_z \quad \forall x \leq 0.5 \tag{36}$$

where:

$$R_x = \begin{bmatrix} 1 & 0 & 0 \\ 0 & \cos\theta & -\sin\theta \\ 0 & \sin\theta & \cos\theta \end{bmatrix}; R_y = \begin{bmatrix} \cos\beta & 0 & \sin\beta \\ 0 & 1 & 0 \\ -\sin\beta & 0 & \cos\beta \end{bmatrix}; R_z = \begin{bmatrix} \cos\delta & -\sin\delta & 0 \\ \sin\delta & \cos\delta & 0 \\ 0 & 0 & 1 \end{bmatrix} \tag{37}$$

with $\theta = \pi/3$, $\beta = \pi/4$ and $\delta = \pi/6$ and:

$$K_2 = \begin{bmatrix} \xi\mathbb{X}^2 + \mathbb{Y}^2 + \mathbb{Z}^2 & -(1-\xi)\mathbb{X}\mathbb{Y} & -(1-\xi)\mathbb{X}\mathbb{Z} \\ -(1-\xi)\mathbb{X}\mathbb{Y} & \mathbb{X}^2 + \xi\mathbb{Y}^2 + \mathbb{Z}^2 & -(1-\xi)\mathbb{Y}\mathbb{Z} \\ -(1-\xi)\mathbb{X}\mathbb{Z} & -(1-\xi)\mathbb{Y}\mathbb{Z} & \mathbb{X}^2 + \mathbb{Y}^2 + \xi\mathbb{Z}^2 \end{bmatrix} \quad \forall x > 0.5 \tag{38}$$

where $\xi = 1000$, $\mathbb{X} = x + \xi^{-1}$, $\mathbb{Y} = y + \xi^{-1}$, $\mathbb{Z} = z + \xi^{-1}$. In Table 4 we present the under and overshoot norms of error for the linear MPFA-D and our new MPFA-DNL. In this table, we can see that, again, the linear version of MPFA-D violates the DMP, returning completely non-physical solutions with strong spurious oscillations for all tested meshes. On the other hand, the MPFA-DNL, even for this highly anisotropic and discontinuous diffusion tensor, keeps the solution between the maximum and the minimum physical bounds for all tested meshes. In Fig. 5, we present the scalar variable field at $y = 0.5$ for the mesh with 15,376 control volumes and again we see that the MPFA-DNL produces a smooth solution

Table 4 Results for the test 4.3—two-halves anisotropic hollow domain

	MPFA-D			MPFA-DNL		
n	$u_{\min}$	$u_{\max}$	ε_m	$u_{\min}$	$u_{\max}$	ε_m
604	− 5.239	6.034	0.607	5.60e−6	1.692	0
4,949	− 102.2	151.7	6.787	0	1.969	0
15,376	− 484.2	295.6	20.62	0	1.992	0

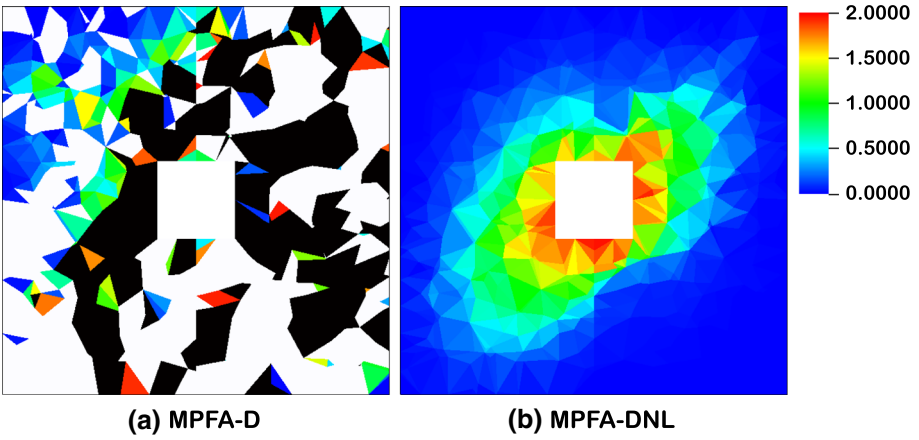

Fig. 5 Scalar variable field on the mesh with 15,376 tetrahedra, at $y = 0.5$, for test 4.3—Two-Halves Anisotropic Hollow Domain. **a** Solution with the linear MPFA-D method. **b** Solution with the new MPFA-DNL. The black regions within the domain indicate overshoots for the scalar variable and the white regions indicate undershoots for the scalar variable

without spurious oscillations even for this test case in which we have a highly anisotropic and heterogeneous diffusion tensor while the linear MPFA-D produces solutions with both, strong under and overshoots for all meshes used.

5 Conclusions

In this paper, we have presented the new MPFA-DNL method, which is a modified nonlinear version of the original linear MPFA-D method of Lira Filho et al. [26]. Our new method was designed to avoid the violation of the Discrete Maximum Principle (DMP) that may occur in MPFA-D solutions, since it is not a monotone scheme, particularly for highly heterogeneous and anisotropic diffusion tensors or distorted meshes. We have modified the original linear MPFA-D through of a flux splitting strategy [15, 16] that splits the flux in a Two-Point Flux Approximation (TPFA) flux contribution and the Cross Diffusion Terms (CDT). Since the latter part is the potential source of spurious oscillations in the scalar field, we perform a flux limiting [18] on the CDT part. These modifications gave us a method which is capable to satisfy the Discrete Maximum Principle eliminating spurious oscillations for the scalar field, even for highly heterogeneous and arbitrary anisotropic diffusion tensors, without harming the convergence rates of the original MPFA-D. Thus, our method is still capable to achieve second order of accuracy on the scalar field and first order on its gradient. In this paper, we restrict ourselves to unstructured tetrahedral meshes, even though, in principle, there is no restriction to extend the method to other polyhedral control volumes.

Acknowledgements The authors thank the Foundation for Support of Science and Technology of Pernambuco (FACEPE), the National Council for Scientific Development (CNPq) and the Coordination for Improvement of Higher Education Personnel (CAPES).

Funding The authors received financial support from some research funding agencies during the preparation of this manuscript, namely the Brazilian Research Council - CNPq (PQ-308334/2019-1, PQ-310242/2018-5 and PQ-310145/2021-0), Foundation for the Support of Science and Technology of Pernambuco - FACEPE (IBPG-1160-3.01/18 and IBPG-0017-3.01/18), and FADE / UFPE / Energi Simulation (Funding No. 53/2020).

Data Availability Enquiries about data availability should be directed to the authors.

Declarations

Conflict of interest The authors have no competing interests to declare that are relevant to the content of this article. All data generated or analyzed during this study are included in this published article. Even so, whoever considers that need additional information, feel free to contact the corresponding author.

References

1. Keilegavlen, E., Aavatsmark, I.: Monotonicity for MPFA methods on triangular grids. Comput. Geosci. **15**, 3–16 (2011). https://doi.org/10.1007/s10596-010-9191-5
2. Aavatsmark, I., Barkve, T., Bøe, O., Mannseth, T.: Discretization on unstructured grids for inhomogeneous, anisotropic media. Part I derivation of the methods. SIAM J. Sci. Comput. **19**, 1700–1716 (1998). https://doi.org/10.1137/S1064827595293582
3. Aavatsmark, I., Barkve, T., Bøe, O., Mannseth, T.: Discretization on unstructured grids for inhomogeneous, anisotropic media. Part II. Discussion and numerical results. SIAM J. Sci. Comput. **19**, 1717–1736 (1998). https://doi.org/10.1137/S1064827595293594
4. Edwards, M.G., Rogers, C.F.: Finite volume discretization with imposed flux continuity for the general tensor pressure equation. Comput. Geosci. **2**, 259–290 (1998). https://doi.org/10.1023/A:1011510505406

5. Fletcher, C.A.J.: Computational Galerkin Methods. Springer, Berlin (1984). https://doi.org/10.1007/978-3-642-85949-6‡‡
6. Ciarlet, P.G.: The finite element method for elliptic problems. Society for Industrial and Applied Mathematics; 2002. https://doi.org/10.1137/1.9780898719208.
7. Raviart, P.A., Thomas, J.M.: A mixed finite element method for 2-nd order elliptic problems. Gall. I., Magenes E. Math. Asp. Finite Elem. Methods. Lect. Notes Math. vol 606., Springer, Berlin, 1977, pp. 292–315. https://doi.org/10.1007/BFb0064470.
8. Durán, R.G.: Mixed finite element methods. Boffi D., Gastaldi L. Mix. Finite Elem. Compat. Cond. Appl. Lect. Notes Math. vol 1939., Springer, Berlin, 2008, pp. 1–44. https://doi.org/10.1007/978-3-540-78319-0_1
9. de Carvalho, D.K.E., Willmersdorf, R.B., Lyra, P.R.M.: Some results on the accuracy of an edge-based finite volume formulation for the solution of elliptic problems in non-homogeneous and non-isotropic media. Int. J. Numer. Methods Fluids **61**, 237–254 (2009). https://doi.org/10.1002/fld.1948
10. Ciarlet, P.G., Raviart, P.-A.: Maximum principle and uniform convergence for the finite element method. Comput. Methods Appl. Mech. Eng. **2**, 17–31 (1973). https://doi.org/10.1016/0045-7825(73)90019-4
11. Korotov, S., Křížek, M., Neittaanmäki, P.: Weakened acute type condition for tetrahedral triangulations and the discrete maximum principle. Math. Comput. **70**, 107–120 (2000). https://doi.org/10.1090/S0025-5718-00-01270-9
12. Burman, E., Ern, A.: Discrete maximum principle for Galerkin approximations of the Laplace operator on arbitrary meshes. Comptes Rendus Math. **338**, 641–646 (2004). https://doi.org/10.1016/j.crma.2004.02.010
13. Le Potier, C.: A nonlinear finite volume scheme satisfying maximum and minimum principles for diffusion operators. Int. J. Finite Vol Inst Mathématiques Marseille, AMU, pp. 1–20 (2009)
14. Cancès, C., Cathala, M., Le Potier, C.: Monotone corrections for generic cell-centered finite volume approximations of anisotropic diffusion equations. Numer. Math. **125**, 387–417 (2013). https://doi.org/10.1007/s00211-013-0545-5
15. Pal, M., Edwards, M.G.: Flux-splitting schemes for improved monotonicity of discrete solutions of elliptic equations with highly anisotropic coefficients. Eur. Conf. Comput. Fluid Dyn. (2006).
16. Pal, M., Edwards, M.G.: Non-linear flux-splitting schemes with imposed discrete maximum principle for elliptic equations with highly anisotropic coefficients. Int. J. Numer. Methods Fluids **66**, 299–323 (2011). https://doi.org/10.1002/fld.2258
17. Chen, Q.-Y., Wan, J., Yang, Y., Mifflin, R.T.: Enriched multi-point flux approximation for general grids. J. Comput. Phys. **227**, 1701–1721 (2008). https://doi.org/10.1016/j.jcp.2007.09.021
18. Kuzmin, D., Shashkov, M.J., Svyatskiy, D.: A constrained finite element method satisfying the discrete maximum principle for anisotropic diffusion problems. J. Comput. Phys. **228**, 3448–3463 (2009). https://doi.org/10.1016/j.jcp.2009.01.031
19. Su, S., Dong, Q., Wu, J.: A decoupled and positivity-preserving discrete duality finite volume scheme for anisotropic diffusion problems on general polygonal meshes. J. Comput. Phys. **372**, 773–798 (2018). https://doi.org/10.1016/j.jcp.2018.06.052
20. Zhao, F., Sheng, Z., Yuan, G.: A monotone combination scheme of diffusion equations on polygonal meshes. ZAMM: J. Appl. Math. Mech./Zeitschrift Für Angew Math Und Mech (2020). https://doi.org/10.1002/zamm.201900320
21. Herbin, R., Hubert, F.: Benchmark on Discretization Schemes for Anisotropic Diffusion Problems on General Grids. Finite Vol. complex Appl. V, pp. 659–692 (2008).
22. Arnold, D.N., Brezzi, F., Cockburn, B., Marini, D.: Discontinuous Galerkin Methods for Elliptic Problems, pp. 89–101 (2000). https://doi.org/10.1007/978-3-642-59721-3_5.
23. Gao, Z., Wu, J.: A linearity-preserving cell-centered scheme for the heterogeneous and anisotropic diffusion equations on general meshes. Int. J. Numer. Methods Fluids **67**, 2157–2183 (2011). https://doi.org/10.1002/fld.2496
24. Contreras, F.R.L., Lyra, P.R.M., Souza, M.R.A., Carvalho, D.K.E.: A cell-centered multipoint flux approximation method with a diamond stencil coupled with a higher order finite volume method for the simulation of oil–water displacements in heterogeneous and anisotropic petroleum reservoirs. Comput. Fluids **127**, 1–16 (2016). https://doi.org/10.1016/j.compfluid.2015.11.013
25. Cavalcante, TdeM., Contreras, F.R.L., Lyra, P.R.M., Carvalho, D.K.E.: A multipoint flux approximation with diamond stencil finite volume scheme for the two-dimensional simulation of fluid flows in naturally fractured reservoirs using a hybrid-grid method. Int. J. Numer. Methods Fluids (2020). https://doi.org/10.1002/fld.4829
26. Lira Filho, R.J.M., Santos, S.R., Cavalcante, TdeM., Contreras, F.R.L., Lyra, P.R.M., Carvalho, D.K.E.: A linearity-preserving finite volume scheme with a diamond stencil for the simulation of anisotropic and

highly heterogeneous diffusion problems using tetrahedral meshes. Comput Struct **250**, 106510 (2021). https://doi.org/10.1016/j.compstruc.2021.106510
27. Sheng, Z., Yuan, G.: Construction of Nonlinear Weighted Method for Finite Volume Schemes Preserving Maximum Principle. SIAM J Sci Comput **40**, A607–A628 (2018). https://doi.org/10.1137/16M1098000
28. Sheng, Z., Yuan, G., Yue, J.: A nonlinear convex combination in the construction of finite volume scheme satisfying maximum principle. Appl. Numer. Math. **156**, 125–139 (2020). https://doi.org/10.1016/j.apnum.2020.04.014
29. Edwards, M.G.: M-matrix flux splitting for general full tensor discretization operators on structured and unstructured grids. J. Comput. Phys. **160**, 1–28 (2000). https://doi.org/10.1006/jcph.2000.6418
30. Zhou, H., Sheng, Z., Yuan, G.: A finite volume method preserving maximum principle for the diffusion equations with imperfect interface. Appl. Numer. Math. **158**, 314–335 (2020). https://doi.org/10.1016/j.apnum.2020.08.008
31. Véron, L.: Elliptic Equations Involving Measures, pp. 593–712 (2004). https://doi.org/10.1016/S1874-5733(04)80010-X.
32. Borsuk, M., Kondratiev, V.: The Dirichlet problem for elliptic linear divergent equations in a nonsmooth domain, 2006, pp. 165–213. https://doi.org/10.1016/S0924-6509(06)80018-8.
33. Aavatsmark, I., Eigestad, G.T., Mallison, B.T., Nordbotten, J.M.: A compact multipoint flux approximation method with improved robustness. Numer. Methods Partial Differ. Equ **24**, 1329–1360 (2008). https://doi.org/10.1002/num.20320
34. Møyner, O., Lie, K.-A.: A multiscale two-point flux-approximation method. J. Comput. Phys. **275**, 273–293 (2014). https://doi.org/10.1016/j.jcp.2014.07.003
35. Eymard, R., Henry, G., Herbin, R., Hubert, F., Klöfkorn, R., Manzini, G.: 3D Benchmark on Discretization Schemes for Anisotropic Diffusion Problems on General Grids, 2011, pp. 895–930. https://doi.org/10.1007/978-3-642-20671-9_89.
36. Queiroz, L.E.S., Souza, M.R.A., Contreras, F.R.L., Lyra, P.R.M., de Carvalho, D.K.E.: On the accuracy of a nonlinear finite volume method for the solution of diffusion problems using different interpolations strategies. Int. J. Numer. Methods Fluids **74**, 270–291 (2014). https://doi.org/10.1002/fld.3850
37. Danilov, A.A., Vassilevski, Y.V.: A monotone nonlinear finite volume method for diffusion equations on conformal polyhedral meshes. Russ J. Numer. Anal. Math. Model (2009). https://doi.org/10.1515/RJNAMM.2009.014